

Large magnetic anisotropy in Fe_xTaS_2 single crystals

G. Wu^{1†}, B. L. Kang¹, Y.-L. Li^{2,3}, T. Wu^{1,5}, N. Z. Wang¹, X. G. Luo¹, Z. Sun^{4,5}, L.-J. Zou², X. H. Chen^{1,5*}

¹Hefei National Laboratory for Physical Science at Microscale and Department of Physics,
and Key Laboratory of Strongly-coupled Quantum Matter Physics, Chinese Academy of Sciences,
University of Science and Technology of China, Hefei, Anhui 230026, China

²Key Laboratory of Materials Physics, Institute of Solid State Physics,
Chinese Academy of Sciences, P. O. Box 1129, Hefei, Anhui 230031, China

³Laboratory for Quantum Design of Functional Materials,
Jiangsu Normal University, Xuzhou, Jiangsu 221116, China

⁴National Synchrotron Radiation Laboratory, University of Science and Technology of China, Hefei, Anhui 230026, China

⁵Collaborative Innovation Center of Advanced Microstructures, Nanjing University, Nanjing 210093, China

In intercalated transition metal dichalcogenide Fe_xTaS_2 ($0.2 \leq x \leq 0.4$) single crystals, large magnetic anisotropy is observed. Transport property measurements indicate that heavy Fe-doping leads to a large anisotropy of resistivity (ρ_c/ρ_{ab}). A sharp M-H hysteresis curve is observed with magnetic field along c-axis, while a linear magnetization appears with magnetic field applied in the ab-plane. The angular dependent magnetic susceptibility from in-plane to out-of-plane indicates that magnetic moments are strongly pinned along the c-axis in an unconventional manner and the coercive field reaches as large as 6 T at T = 5 K. First-principles calculation clearly suggests that the strong spin-orbital coupling give rise to such a large anisotropy of magnetism. The strong pinning effect of magnetic moments along c-axis makes this material a very promising candidate for the development of spin-aligner in spintronics devices.

PACS numbers: 75.30.Cr, 75.30.Gw, 75.50.-y

Transition metal dichalcogenides have been subject to intensive study due to their rich physical properties as a result of strong electron correlation and electron-phonon coupling. These intriguing compounds share the same characteristics that they are all low dimensional with layered structures, and receptive to intercalation due to van der Waals force between S-M-S layers[1–3]. In this family, people have discovered charge density wave (CDW) order in $1T-TaS_2$ [4], long range magnetic order in Mn_xTaS_2 (ferromagnetism)[5] and Fe_xTiSe_2 (antiferromagnetism)[6], and superconductivity in K_xTiSe_2 and Cu_xTiSe_2 [7–9]. Among them, iron-intercalated $1T-TaS_2$ compounds have been greatly attractive owing to their exotic magnetic properties originating from the interaction between crystal field, electron orbit and local moment of Fe^{2+} .

Previous works by Cava *et al.*[10] and Ong *et al.*[11] have shown that in Fe_xTaS_2 ($x = 1/4$) Fe^{2+} ions are distributed periodically in a doubled cell of parent compound TaS_2 rather than randomly scattered between TaS_2 layers. Computational results has validated the ferromagnetic transition for $x = 0.33$ [12]. In Fe_xTaS_2 system, the magnetic properties of Fe_xTaS_2 change from spin glass ($x < 0.2$) to ferromagnetism ($0.2 \leq x \leq 0.4$)[13] and antiferromagnetism ($x > 0.4$)[17] with the increasing of x . For $0.20 \leq x \leq 0.40$, the Curie temperature T_c is non-monotonous with x , $T_c = 90$ K for $x = 0.2$; $T_c = 163$ K for

$x = 0.26$; $T_c = 55$ K for $x = 0.34$ [13]. The Curie temperature decreases as x further increases. Cheong *et al.* suggested the nano domains and unquenched orbital moment contribute to the large magnetic anisotropy and magnetoresistance, respectively [14, 15]. However, Morosan *et al.* attributed the large magnetoresistance to disorder [16]. A systematical study on the magnetic and transport properties of Fe_xTaS_2 , especially the magnetization and transport behaviors under different magnetic fields, are critical to reveal the intrinsic properties of this material. In this paper, we present the large magnetic anisotropy in the resistivity, magnetic susceptibility and magnetization in Fe_xTaS_2 single crystals and elucidate the microscopic origin of such a huge magnetic anisotropy.

The Fe_xTaS_2 ($0.2 \leq x \leq 0.40$) single crystals were grown by the chemical iodine vapor transport method. Fe (>99.5%), Ta (>99.5%) and S (>99.5%) element powders were mixed and thoroughly ground, then pressed into pellets. The pellets were sealed under vacuum ($< 1.0 \times 10^{-2}$ Pa) in a quartz tube ($\phi 13\text{mm} \times 150\text{mm}$) with a small quantity of iodine ($10\text{mg}/\text{cm}^{-3}$). The tube was slowly heated to 1000°C in 400 minutes, and the cold end of the tube was kept at 950°C . After ten days, the furnace was cooled to room temperature over a few hours. Finally many high quality plate-like Fe_xTaS_2 single crystals were obtained. The single crystals were black and the typical dimension is about $3 \times 3 \times 0.3\text{mm}^3$.

Figs. 1(a) and (b) demonstrates how the resistivity anisotropy evolves with Fe doping. As the dopant Fe increases from 0.2 to 0.4, the electronic resistivity in the ab-plane significantly decreases, while the out-of plane resistivity increases drastically, thus leading to an en-

*Corresponding author; Electronic address: chenxh@ustc.edu.cn; † Present address: Oxford Instruments(Shanghai) Co., Ltd, Shanghai 200233, China

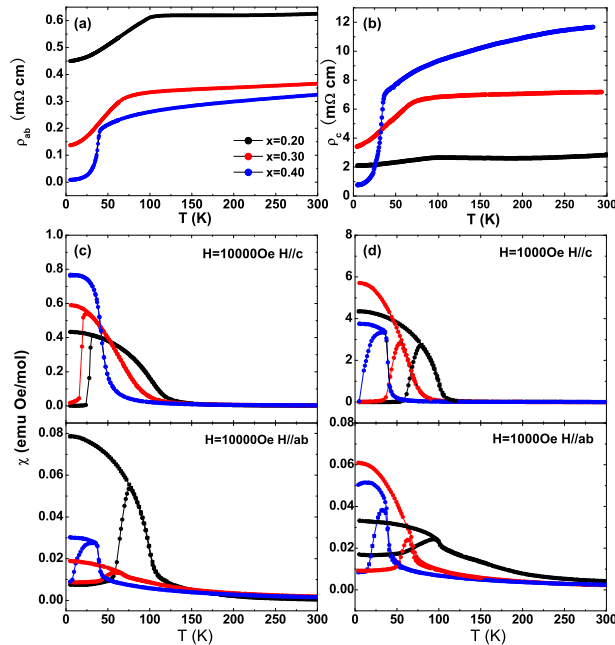


FIG. 1: (Color online) (a): Temperature dependence of in-plane resistivity; (b): Temperature dependence of out-of-plane resistivity; (c): Temperature dependence of magnetic susceptibility under the magnetic field of 1 Tesla applied along in-plane and out-of plane, respectively; (d): Temperature dependence of magnetic susceptibility under the magnetic field of 0.1 Tesla applied along in-plane and out-of plane, respectively. The data were obtained from the Fe_xTaS_2 single crystals with $x = 0.2$ (black), 0.3 (red) and 0.4 (blue).

hanced anisotropy of ρ_c/ρ_{ab} . The ferromagnetic phase transition indicated by the kinks in resistivity is gradually suppressed with Fe doping, from 105 K for $x=0.2$, to 76 K for $x=0.3$, and 43 K for $x=0.4$, respectively. Figs. 1(c) and (d) show the temperature dependence of magnetic susceptibility with the applied magnetic field of 10000 Oe and 1000 Oe, respectively. The in-plane susceptibility is significantly smaller than the c-axis susceptibility, unambiguously indicating that the easy axis is perpendicular to the ab-plane, and a large field tends to reduce such magnetic anisotropy. It should be pointed out that the zero field cooled magnetization curve with the magnetic field applied along c-axis reaches almost zero below T_c , while magnetization with the magnetic field applied in the ab-plane can not yields zero susceptibility below T_c . This contrast implies that there exists an anisotropic magnetic energy between the ab-plane and c-axis. These results are consistent with those reported in Ref. [13]

Fig. 2(a) shows the magnetization loops at different temperatures under the magnetic field applied along c-axis of $Fe_{0.2}TaS_2$. Clear M-H loops shows up below the Curie temperature with the external magnetic field ap-

plied along the c-axis. The coercive field systematically decreases with increasing the temperature. The most striking features are the large coercive field up to 6 T at 5 K and the sharp magnetic transition to reach saturation magnetization (M_s). Fig. 2(b) shows the evolution of the magnetization (M_{ab}) with the external magnetic field applied in ab-plane at different temperatures. There is no M-H loop at 5 K, and the magnetization M_{ab} increases linearly with the magnetic field up to 7 T with a small slope. This behavior suggests that the pinning force along c-axis is so strong at 5 K that only statistical net moment could be observed in the ab-plane magnetization (M_{ab}). When temperature rises to 60 K, the magnetic anisotropy decreases and more local moments from Fe ions are aligned in the ab-plane to form domain, so that a skew M-H loop appears during the magnetizing process as shown in Fig. 2(b). Such a behavior implies that the in-plane magnetic crystal energy is weaker than that along c-axis. As temperature rises to above T_c , the thermal fluctuation becomes dominant, and the magnetization correspondingly follows a linear dependence of the magnetic field and shows a paramagnetic behavior. As shown in Fig. 2(a), the slope of the linear magnetic field dependent M_{ab} is so small that the anisotropy field H_A approximately exceeds 60 T if we extrapolate the linear M_{ab} to the saturation value of M_c . Therefore, the first order anisotropic coefficient $K_1 = \mu_0 M_s H_A / 2$ is estimated to be about 6.5 meV. As temperature increases, the coercive field and remaining magnetization shrink quickly, suggesting a rapid decrease of K_1 .

Fig. 2(c) shows the evolution of magnetization loop with the direction of external magnetic field at $T = 25$ K. A continuous 'flattened' loop is observed, and the saturated magnetization continuously decreases and the coercive field monotonously increases with the variation of the applied magnetic field from along the c-axis to the in-plane. The switching field H_s of the magnetization obtained from Fig. 2(c) are plotted in Fig. 2(d), and the evolution of H_s with the direction of the applied magnetic field can be well fitted by the formula $H_s = 1.156 / \cos(\theta)$. This behavior indicates that $Fe_{0.2}TaS_2$ is almost an ideal single domain ferromagnetic system with the easy axis perpendicular to the ab-plane.

In order to quantify the pinning strength in this system, angle-dependent magnetization and magnetoresistance with the direction of external magnetic field varying from c-axis to ab-plane were carried out, and the results are shown in Fig. 3. As shown in Fig. 3(a), the applied external field up to 5 Tesla still cannot flip the spins at $T = 2$ K, so that the magnetization behaves exactly in a sinusoid way. As the external magnetic field rises to 6.5 and 7 Tesla, there are clear jumps on magnetization at 155° and 140° relative to c-axis, respectively. In Fig. 3(c), similar behavior persists at $T = 15$ K. The magnetic field up to 1 T can not flip the spins, while the spin flip takes place with increasing the field up to

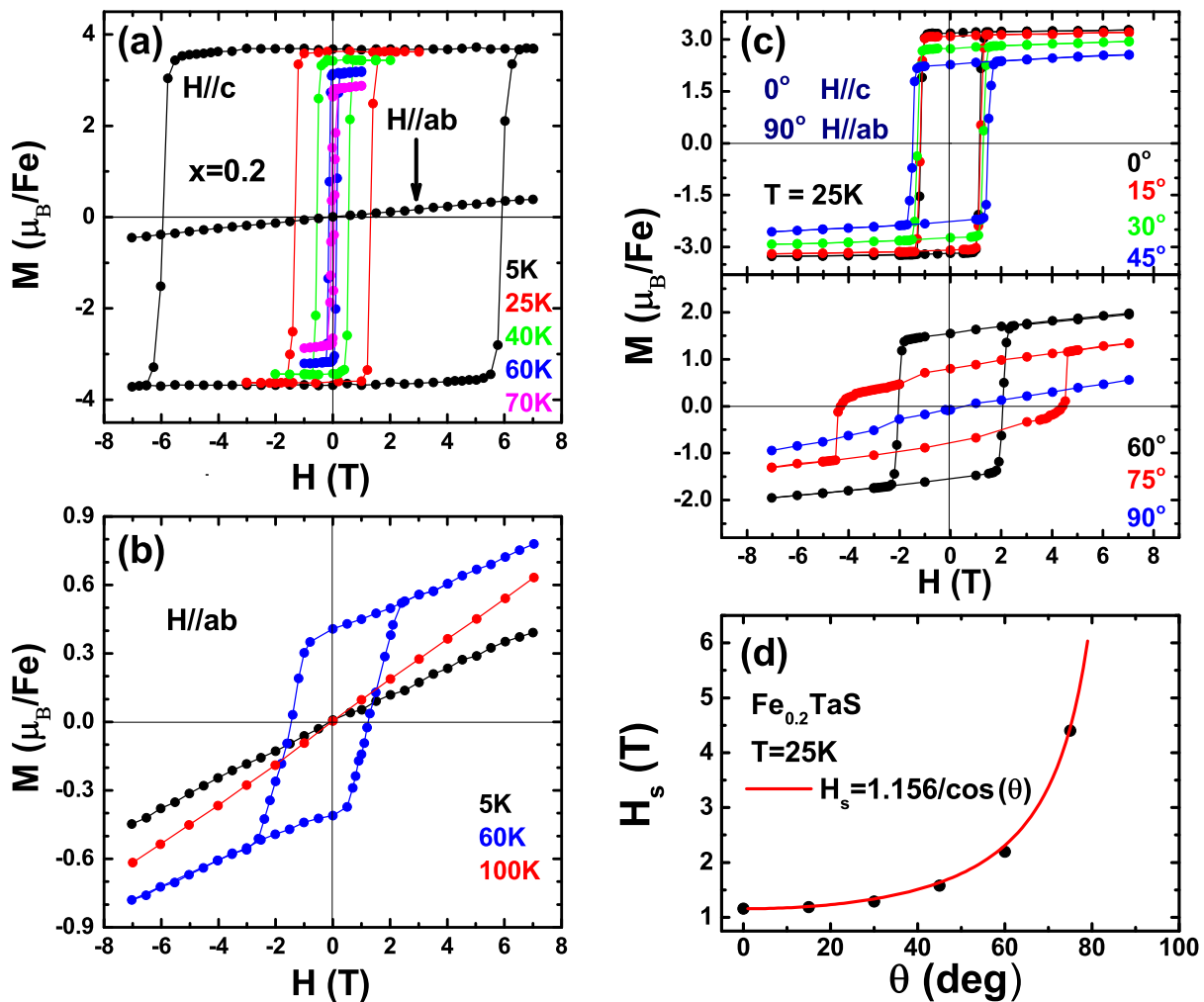


FIG. 2: (Color online) Temperature dependence of M-H loop in $Fe_{0.2}TaS_2$ with the external magnetic field applied (a) along c-axis and (b) in ab-plane. (c): M-H loops at 25 K in $Fe_{0.2}TaS_2$ with the external magnetic field applied along different directions from c-axis to ab-plane. (d): The angle-dependent the switching field H_s of magnetization. The red curve is the fitting data obtained by the formula $H_s = 1.156/\cos(\theta)$.

3 Tesla. Our data indicates that the *critical field* of the spin flip decreases with increasing temperature. A pictorial explanation is sketched in Fig. 3(a). The spins of Fe ions are pinned along c-axis at low temperature. When the external magnetic field is rotated, the spin alignment holds until the magnetic energy $\mu H \cos(\theta)$ surpasses the pinning energy E_p , then an 180-degree flip happens for all spins, leading to the sharp jump of magnetization from negative (positive) to positive (negative). Based on the critical angle of the spin flip at certain magnetic field, we can estimate the pinning energy in terms of following relation:

$$E_p = -\mu H \cos(\theta) \quad (1)$$

which could be verified for both of the cases at 2 K and 15 K, respectively. The pinning energy E_p is ~ 1.24 meV at 2 K, and ~ 0.53 meV at 15 K. E_p gradually decreases with increasing temperature due to thermal fluctuation. Simi-

lar magnetoresistance measurement confirms the spin flip under rotating external field from the c-axis to the ab-plane, as shown in Figs. 3(b) and 3(d). The flipping critical angle is exactly the same as those obtained from the angle-dependent magnetization. These results not only confirm the existence of pinning along the c-axis, but also suggest that magnetic scattering is profound in this system. Moreover, as temperature rises, the sharp jump in magnetization become weak and finally disappears, closely correlated with the behavior of magnetoresistance. Such a correlation indicates that the magnetic scattering is an indispensable component in the electronic transport and there exists a strong spin-electron coupling.

The key to the understanding of these exotic phenomena in Fe_xTaS_2 system is to clarify the roles of Fe spins and its coupling with environment. In conventional 3d transition metals, the orbital angular momentum is

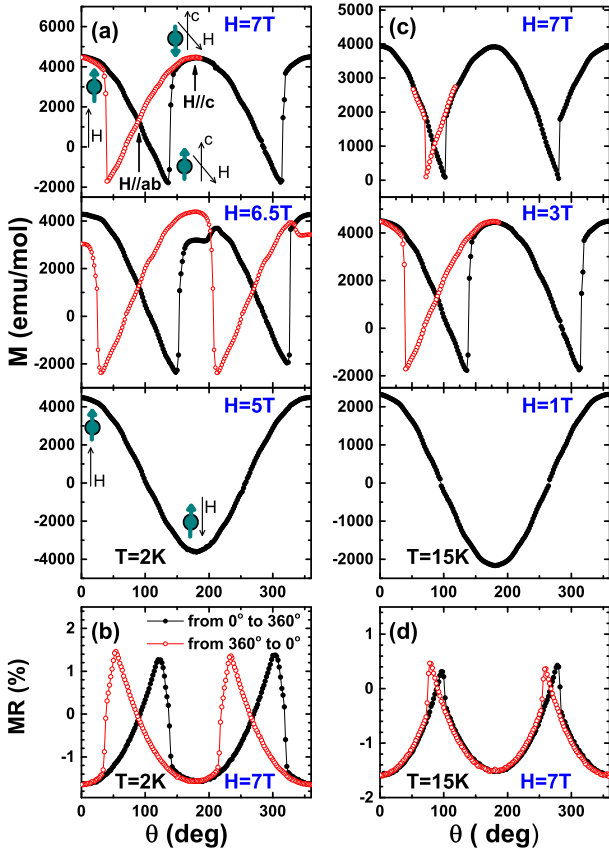


FIG. 3: (Color online) Angle-dependent magnetization under different magnetic fields by tuning the external magnetic field from along c -axis to in the ab -plane for $Fe_{0.25}TaS_2$ single crystal at (a): 2 K (c): 15 K. The green dot and arrow represent the direction of totally local moment of Fe ions. Angle-dependent magnetoconductance under the magnetic field of 7 Tesla by tuning the magnetic field from along c -axis to in the ab -plane for $Fe_{0.25}TaS_2$ single crystal at (a): 2 K (c): 15 K. The angle of 0° represents the direction of magnetic field along c -axis direction, while the angle of 90° means the magnetic field in ab -plane. The black data are obtained by tuning the H from 0° to 360° while the red data are obtained by tuning the H from 360° to 0° . The black and red data show a perfect symmetry relative to ab -plane.

partially or almost fully quenched due to the complete or partial lift of the orbital degeneracy in 3d electronic states, as a result of the presence of low symmetric crystal field. In the present case, our theoretical calculations and analysis show that the intercalated Fe ions are coordinated in a triangular crystalline field of six S ions, the orbital degeneracy of Fe 3d orbitals is partially removed. A crystal field separates the upper two-fold e_g levels from lower three-fold degenerate t_{2g} levels with Δ_{CF} of 1 eV. This leads to an effective orbital angular momentum $L = 1$, in agreement with Cheong *et al.*'s result [14]. Considering the Fe spin of $S=2$ in the Fe 3d⁴ configuration, we have the total angular momentum of $J = 3$ for Fe ions. Therefore, the theoretical value of magnetic mo-

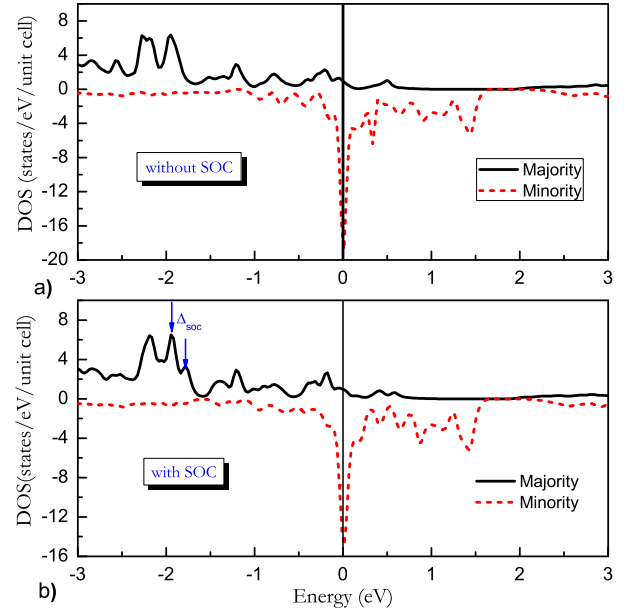


FIG. 4: (Color online) The spin-polarized density of states (DOS) in $Fe_{0.25}TaS_2$, calculated without (a) and with (b) spin-orbit coupling. The DOS near the Fermi energy is highly spin-polarized, with dominant $d_{x^2-y^2}$ electrons. The arrows in (b) indicate the energy splitting caused by the spin-orbit coupling.

ment in Fe^{2+} is about $5 \mu_B$, in good agreement with our and Cava *et al.*'s [10] experimental results. In order to find out the origin of strong pinning of spin alignment along c -axis, we have carried out further first-principles electronic structure calculation, and found considerable effect from the spin-orbital coupling, as shown in Fig. 4. By comparing the density of states (DOS) without and with the spin-orbital coupling, one may find that the spin-orbital coupling brings about a 0.05 eV splitting in the $d_{x^2-y^2}$ orbital around 2 eV below the Fermi level (see Figs. 4(a) and 4(b)). The strongly spin-polarized Fermi surface also directly gives rise to the strong field-dependent transport properties. At last, we could infer the magnetic anisotropy parameter to be

$$K_1 = \frac{25\lambda^2}{9\Delta_{CF}} \simeq 7meV \quad (2)$$

which decently agrees with the experimental data of ~ 6.5 meV. We also notice that a recent work suggested the crucial role of electronic correlation [18]. The first-principles electronic structure calculation confirms that the spin-orbital coupling can induced large magnetic anisotropy and strong spin pinning along c -axis in Fe_xTaS_2 , the calculated magnetic anisotropy energy K_1 is well consistent with the experiment result.

Efficient electrical injection of spin-polarized carriers from a contact into a semiconductor is one of the essential requirements to utilize carrier spin as an operational paradigm for future electronic devices like a spin-

LED[19–21]. Two kinds of spin aligner are used to polarize the spin of the carriers. One is diluted magnetic semiconductor and the other is ferromagnetic metal. The large coercive field and the sharp transition in the *c*-axis magnetization of Fe_xTaS_2 can provide as the spin aligner in electrical spin injection in spintronics.

In summary, we have observed large magnetic anisotropy in Fe_xTaS_2 system. Coercive field as large as 6 T and sharp transition exist in *c*-axis magnetization. Angle-dependent magnetization at different temperatures from *ab*-plane to *c*-axis reveals that the strong pinning along *c*-axis fits the simple spin-flip model, in favor of the single domain picture[10]. Theoretical analysis suggests that the magnetic anisotropy comes from the spin-orbital coupling of Fe ions in the triangular crystal field. Both of first-principles electronic structure calculation and experiment indicate a magnetic anisotropy energy of ~ 7 meV. Our data suggests that Fe_xTaS_2 can serve as a spin aligner in electrical spin injection in spintronics[19]. The spontaneous strong spin polarization in this material can also be adopted as a reliable spin current source.

-
- [1] M. S. Whittingham, *Prog. Solid State Chem.* **12**, 41 (1978).
- [2] M. S. Whittingham, *J. Electrochem. Soc.* **123**, 315 (1976).
- [3] L. Trichet, J. Rouxel, and M. M. Pouchard, *J. Solid State Chem.* **14**, 283 (1975).
- [4] D. R. Karczewski, and B. P. Clayman, *Phys. Rev. B* **19**, 6367 (1979).
- [5] S. S. P. Parkin and R. H. Friend, *Phil. Mag.* **41** 65 (1980).
- [6] M. A. Buhannic, P. Colombet, M. Danot, and G. Calvarin, *J. Solid State Chem.* **69**, 280 (1987).
- [7] A. Schlicht, M. Schwenker, W. Biberacher, and A. Lerf, *J. Phys. Chem. B* **105**, 4867 (2001).
- [8] E. Morosan, H. W. Zandbergen, B. S. Dennis, J. W. G. Bos, Y. Onose, T. Klimczuk, A. P. Ramirez, N. P. Ong, and R. J. Cava, *Nat. Phys.* **2**, 544 (2006).
- [9] G. Wu, H. X. Yang, L. Zhao, X. G. Lou, T. Wu, G. Y. Wang, and X. H. Chen, *Phys. Rev. B* **76**, 024513 (2007).
- [10] E. Morosan, H. W. Zandbergen, Lu Li, Minhyea Lee, J. G. Checkelsky, M. Heinrich, T. Siegrist, N. P. Ong, and R. J. Cava, *Phys. Rev. B* **75**, 104401 (2007).
- [11] J. G. Checkelsky, M. H. Lee, E. Morosan, R. J. Cava, and N. P. Ong, *Phys. Rev. B* **77**, 014433 (2008).
- [12] J. Dijkstra, P. J. Zijlema, C. F. van Bruggen, C. Haas, and R. A. de Groot, *J. Phys.: Condens. Matt.* **1**, 6363 (1989).
- [13] M. Eibschütz, S. Mahajan, F. J. DiSalvo, G. W. Hull, and J. V. Waszczak, *J. Appl. Phys.* **52**, 2098 (1981).
- [14] K.-T. Ko, K. Kim, S. B. Kim, H.-D. Kim, J.-Y. Kim, B. I. Min, J.-H. Park, F.-H. Chang, H.-J. Lin, A. Tanaka, and S.-W. Cheong, *Phys. Rev. Lett.* **107**, 247201 (2011).
- [15] Y. J. Choi, S. B. Kim, T. Asada, S. Park, W. D. Wu, Y. Horibe, and S.-W. Cheong, *Europhys. Lett.* **86**, 37012 (2009).
- [16] C.-W. Chen, S. Chikara, V. S. Zapf, and E. Morosan, *Phys. Rev. B* **94**, 054406 (2016).
- [17] H. Narita, H. Ikuta, H. Hinode, T. Uchida, T. Ohtani, and M. Wakihara, *J. Solid State Chem.* **108**, 148 (1994).
- [18] V. Loganathan, J.-X. Zhu, and A. H. Nevidomskyy, *arXiv:1605.07141* (2016).
- [19] R. Fiederling, M. Keim, G. Reuscher, W. Ossau, G. Schmidt, A. Waag, and L. W. Molenkamp, *Nature* **402**, 787 (1999).
- [20] A. T. Hanbicki, B. T. Jonker, G. Itskos, G. Kioussoglou, and A. Petrou, *Appl. Phys. Lett.* **80**, 1240 (2002).
- [21] B. L. Liu, M. Senesa, S. Couderca, J. F. Boboa, X. Mariea, T. Amanda, C. Fontaine, and A. Arnoult, *Physica E*, **17**, 358 (2003).

Acknowledgements This work is supported by the National Key R&D Program of the MOST of China (Grant No. 2016YFA0300201), the Nature Science Foundation of China (Grant No: 11474287), Hefei Science Center CAS (2016HSC-IU001) and the “Strategic Priority Research Program” of the Chinese Academy of Sciences (grant no. XDB04040100).